



The possible physical mechanism for the EAP–SR co-action

Zhiqiang Gong¹ · Guolin Feng¹ · Muhammad Mubashar Dogar^{2,3} · Gang Huang⁴

Received: 13 October 2016 / Accepted: 10 October 2017 / Published online: 17 November 2017
© Springer-Verlag GmbH Germany 2017

Abstract

The anomalous characteristics of summer precipitation and atmospheric circulation in the East Asia–West Pacific Region (EA–WP) associated with the co-action of East Asia/Pacific teleconnection–Silk Road teleconnection (EAP–SR) are investigated in this study. The compositions of EAP–SR phase anomalies can be expressed as pattern I (+ +), pattern II (+ –), pattern III (– –), and pattern IV (– +) using EAP and SR indices. It is found that the spatial distribution of summer precipitation anomalies in EA–WP corresponding to pattern I (III) shows a tripole structure in the meridional direction and a zonal dipole structure in the subtropical region, while pattern II (IV) presents a tripole pattern in meridional direction with compressed and continuous anomalies in the zonal direction over the subtropical region. The similar meridional and zonal structures are also found in the geopotential height anomalies at 500-hPa, as well as wind anomalies and moisture convergence at 850-hPa. Finally, a schematic mechanism for the EAP–SR co-action upon the summer precipitation in EA–WP is built: (1) Pattern I (III) exhibits that the negative (positive) sea surface temperature (SST) anomalies over tropical East Pacific may cause the enhanced (weakened) convective activity dominating the West Pacific, trigger the positive (negative) EAP teleconnection and produce more (less) precipitation. Besides, the negative (positive) SST anomalies over the Indonesia Maritime Continent (IMC) may further weaken (strengthen) anomalous downward (upward) motion over the South China Sea (SCS), cause negative (positive) geopotential height anomalies at the middle troposphere and surrounding regions through the function of the tropical Hadley circulation. Then the negative (positive) geopotential height anomalies could motivate the positive (negative) EAP teleconnection through the northward propagation of wave-activity perturbation. Meanwhile, a positive (negative) geopotential height anomalous pattern over Eastern Europe motivates a Rossby wave train propagation from Western Europe to west-central Asia. This circumstance can cause suppressed (enhanced) convection and less (more) precipitation over northwestern India and Pakistan, which could strengthen the negative (positive) geopotential height and positive (negative) vorticity anomalies over central East Asia, resulting in a negative (positive) SR teleconnection along the Asian jet stream. A positive (negative) lobe over the Korean Peninsula and Japan corresponding to SR overlaps with a positive (negative) lobe of EAP, which strengthens the anomalous phase contrast on both sides of 120°E. Accordingly, summer precipitation anomalies in EA–WP exhibit the meridional tripole pattern and the zonal dipole pattern. (2) Pattern II (IV) indicates that the normal SST anomalies over the tropical East Pacific cause the weak tele-impact on the tropical West Pacific, while the positive (negative) SST anomalies over the IMC will lead to a negative (positive) lobe of EAP over the subtropical region. This circumstance can weaken the positive (negative) lobe of SR over subtropical region, causing compressed and continuous negative (positive) anomalies of 500-hPa geopotential height and positive (negative) surface precipitation anomalies from central East China to Japan.

Keywords East Asia/Pacific teleconnection · Silk Road teleconnection · Co-action · Precipitation

1 Introduction

The East Asian Summer Monsoon (EASM) is an important subsystem of the global climate system. The EASM has obvious interannual variability and causes severe droughts and floods in China, the Korean peninsula, Japan and many other parts of East and South Asia (Nitta and Hu 1996;

✉ Gang Huang
gq0929@126.com

Extended author information available on the last page of the article

Huang et al. 1998; Wang et al. 2001). Therefore, the interannual variability of the EASM, especially the spatial and temporal variability of summer precipitation over East Asia, has always been an imperative research task deserving interest and attention from meteorologists involved in climate diagnosis and prediction (Webster and Yang 1992; Huang et al. 1993; Yang and Lau 2004; Gong et al. 2015b). Studying the leading teleconnection modes and associated climatic impacts are important for better understanding of the global and regional climate system, especially the South Asian and the East Asian monsoon systems (Dogar et al. 2017).

Summer precipitation over the East Asia–West Pacific region (EA–WP) is influenced by the northwestern Pacific subtropical high (PASH), which is part of the EASM system. The northward movement and westward extension of PASH influences the moisture transportation from low latitude to mid-high latitude areas. They cause anomalous convective activities over the northwestern Pacific and coastal areas that trigger severe drought and flooding events in EA (Huang et al. 1998; Ding and Chan 2005; Li et al. 2008). The PASH is characterized by interactions among its components in the meridional direction (Lu 2004), i.e., either the East Asia–Pacific (EAP) teleconnection (Huang 1987) or the Pacific–Japan (PJ) teleconnection (Nitta 1987) plays an important role in mediating influence of PASH on summertime climate in EA–WP. The obvious meridional tripole pattern from the tropics pole-ward to the extra-tropics, triggered by anomalies of convective activities over the tropical western Pacific, causes the summertime moisture transportation fluxes and precipitation in East Asia. This mechanism presents the corresponding tripole pattern on different time scales (Huang et al. 2012a). The EAP pattern has been used to explain the internal process of the meridional tripole pattern of the spatial and temporal variability of the EASM system on interannual and interdecadal scales (Huang et al. 2006, 2012b). Accordingly, the spatial distributions of summertime drought and flood events over East Asia have a similar characteristic of the meridional tripole pattern as the EAP teleconnection (Huang et al. 2007).

Meanwhile, the Silk Road (SR) teleconnection (Enomoto et al. 2003), as a wave-like pattern observed from the meridional wind field at 200 hPa, is another dominant teleconnection pattern that influences summer climate in EA–WP. SR especially influences the interannual variability of PASH from the zonal direction (Takaya and Nakamura 2001; Kosaka et al. 2009; Chen et al. 2013). Ding and Chan (2005) suggests that the propagation of the Rossby wave train along the jet stream across the Eurasian continent to East Asia at the upper levels may influence the south-northward advance and retreat of the summer PASH. This process may further influence the onset and offset date of the summer precipitation season over East Asia (Feng et al. 2013; Gong et al. 2015a, 2016). Kosaka et al. (2012) also revealed that the

SR pattern, another dominant teleconnection that influences the northwestern PASH and East Asia, is unpredictable at monthly to seasonal leading time scale, limiting the seasonal predictability of summer precipitation in East Asia.

Based on the above discussion, the meridional pattern of summer precipitation anomalies over EA–WP has correlations with both EAP and SR teleconnections. Furthermore, Lu (2004) revealed that the interaction of SR with EAP modulates the EAP teleconnection exhibiting an intraseasonal difference between early summer and late summer. Kosaka et al. (2012) analyzed the interference of SR teleconnection to the anomalous summer climate of 2010 in East Asia. These studies imply that the EAP teleconnection pattern can be modulated by the SR teleconnection. Hsu and Lin (2007) further presented the relationship of the tripole summer precipitation pattern with both PJ and SR teleconnections and revealed that the PJ teleconnection is more evident in the positive phase of summer precipitation, while the SR pattern is more evident in the negative phase.

In view of the above statement, although the EAP and SR patterns have been revealed, the mechanism of co-action of EA and SR on influencing the precipitation anomalous pattern in EA–WP is still obscure. For example, there are still remaining questions such as (1) along with the meridional tripole pattern, is there any other zonal pattern of summer precipitation caused by the co-influence of EAP and SR, and (2) if so, what are internal processes and external forces leading to the zonal anomalous pattern? Therefore, it is worthwhile to explore atmospheric circulation and precipitation anomaly patterns in EA–WP originating from different EAP–SR compositions, and the relevant physical mechanism.

In this study, we use the EAP index (Huang 2004) and a defined SR index to identify their probable compositions in different phases. Then, the distinct anomalous patterns of precipitation and atmospheric circulation in EA–WP of EAP–SR compositions, which remained unnoticed in previous studies, are presented in Sect. 3. In Sect. 4, we discuss the possible physical mechanism of EAP and SR compositions through the analysis of thermal convective activity and wave-activity propagation. The SST anomalies and wave patterns corresponding to EAP–SR compositions are presented in Sect. 5. Finally, conclusions and brief discussions are given in Sect. 6.

2 Data and method

Atmospheric circulation data used in this study includes the monthly data from NCEP re-analysis in terms of the geopotential height, wind, omega, specific humidity at different levels from 1979 to 2015 (Masao et al. 2002). Data of Outgoing Long wave Radiation (OLR) and surface pressure

from 1979 to 2015 is also from NCEP re-analysis. The CPC merged analysis of precipitation (CMAP) monthly precipitation observation dataset from 1979 to 2015 is interpolated to a horizontal resolution of $2.5^\circ \times 2.5^\circ$. The reconstructed monthly global sea surface temperature (SST) dataset from 1979 to 2015 is COBE SST produced by Japan Meteorological Administration (Ishii et al. 2005).

The EAP teleconnection index (Huang 2004) is defined in formula (1),

$$I_{EAP} = -0.25Z'(60^\circ N, 125^\circ E) + 0.5 Z'(40^\circ N, 125^\circ E) - 0.25 Z'(20^\circ N, 125^\circ E) \tag{1}$$

where $Z' = \sin 45 / \sin \varphi (Z - \bar{Z})$ is the standardized seasonal mean 500 hPa anomaly at a grid point with the latitude φ .

Similar to the definition of EAP index, the SR teleconnection index is defined in formula (2),

$$I_{SR} = -0.25V'(40^\circ N, 80^\circ E) + 0.5 V'(40^\circ N, 110^\circ E) - 0.25 V'(40^\circ N, 140^\circ E) \tag{2}$$

where $V' = \sin 45 / \sin \varphi (V - \bar{V})$ is the standardized seasonal mean meridional wind velocity anomaly of a grid point with the latitude φ at the level 200-hPa.

The vertically integrated moisture flux (Q) in the troposphere from the surface to 200-hPa is calculated by:

$$\vec{Q} = \frac{1}{g} \int_{200}^{p_s} q \vec{V} dp \tag{3}$$

where g , q , V , and p_s are the acceleration of gravity, specific humidity, horizontal wind vector, and surface pressure, respectively (Li et al. 2012).

In order to validate whether indices of EAP and SR well represent the two teleconnection patterns, correlation coefficients (CCs) of EAP and SR indices, along with other existing indices representing the same teleconnection pattern, are presented in Table 1. Most CCs are above the 95% significance level. The correlation coefficient (Kosaka et al. 2013) of the EAP index defined as proposed by Huang (2004), has a CC 0.58 with PC-1_{Z500} reaches 0.58, indicating that the EAP index of this study could reflect the precipitation features over East Asia. Since the

circumglobal teleconnection index (CGTI) suggested by Ding and Wang (2005) and Ding et al. (2011) could well explain precipitation anomalies over the subtropical region in the northern hemisphere, CC of SR index with CGTI reaches 0.62, implying that the SR index defined in the study could reflect the SR teleconnection.

Note, Indices compared with EAP include the first principle component of 500-hPa height (PC-1_{Z500}) over the region (10°N–70°N, 90°E–160°E), the PC2 of the north hemispheric 200-hPa geopotential height anomalies (PC-2_{Z200}) (Ding et al. 2011), the PC3 of the 200-hPa height (PC-3_{Z200}) over the region (0–80°N, 70°E–160°E), the western Pacific–North America teleconnection index (WNPSMI) defined as the meridional shear of the 850-hPa westerly, in terms of the 850-hPa zonal winds averaged over the southern region (5°N–15°N, 100°E–130°E) minus that averaged over the northern region (20°N–30°N, 110°E–140°E) (Wang et al. 2001). Indices compared with SR include the first principle component of 200-hPa meridional wind field (PC-4_{V200}) and 200-hPa height (PC-5_{Z200}) field over the region (20°N–60°N, 30°E–160°E), and the circumglobal teleconnection pattern index (CGTI) defined by average of the 200-hPa geopotential height over the region (35°N–40°N, 60°E–70°E) (Ding and Chan 2005).

The formula (4) is used to calculate the wave-activity flux W in pressure (p) coordinates (Hoskins and Karoly 1981; Gong et al. 2013; Qiao et al. 2015):

$$W = \frac{1}{2|\vec{U}|} \left(\begin{aligned} & \bar{u} \left[\left(\frac{\partial \Psi'}{\partial x} \right)^2 - \Psi' \frac{\partial^2 \Psi'}{\partial x^2} \right] + \bar{v} \left[\frac{\partial \Psi'}{\partial x} \frac{\partial \Psi'}{\partial y} - \Psi' \frac{\partial^2 \Psi'}{\partial x \partial y} \right] \\ & \bar{u} \left[\frac{\partial \Psi'}{\partial x} \frac{\partial \Psi'}{\partial y} - \Psi' \frac{\partial^2 \Psi'}{\partial x \partial y} \right] + \bar{v} \left[\left(\frac{\partial \Psi'}{\partial y} \right)^2 - \Psi' \frac{\partial^2 \Psi'}{\partial y^2} \right] \\ & \frac{f_0^2}{R\sigma/p} \left\{ \bar{u} \left[\frac{\partial \Psi'}{\partial x} \frac{\partial \Psi'}{\partial p} - \Psi' \frac{\partial^2 \Psi'}{\partial x \partial p} \right] + \bar{v} \left[\frac{\partial \Psi'}{\partial y} \frac{\partial \Psi'}{\partial p} - \Psi' \frac{\partial^2 \Psi'}{\partial y \partial p} \right] \right\} \end{aligned} \right) \tag{4}$$

where Ψ is the stream-function, f the Coriolis parameter, R the gas constant, $U = (u, v)$ the horizontal wind velocity, and $\sigma = \frac{RT}{C_p P} - dT/dp$, with temperature, T and the specific heat

at constant pressure, C_p . Over bars and primes denote basic-state quantities and perturbations, respectively. Analysis of this study in terms of precipitation, circulations, EAP and SR teleconnections are conducted for the summertime (June, July and August, JJA).

3 EAP and SR teleconnection and corresponding composition patterns

Figure 1a shows the first spatial mode (with 30.2% contribution to total variance) extracted through an empirical orthogonal function (EOF) analysis applied to interannual

Table 1 Correlation coefficients of EAP index and SR index with other similar indices

	EAP		SR
PC-1 _{Z500}	0.58	PC-4 _{V200}	0.88
PC-2 _{Z200}	0.32	CGTI	0.62
PC-3 _{Z200}	0.52	PC-5 _{Z200}	0.26
WNPSMI	0.36		

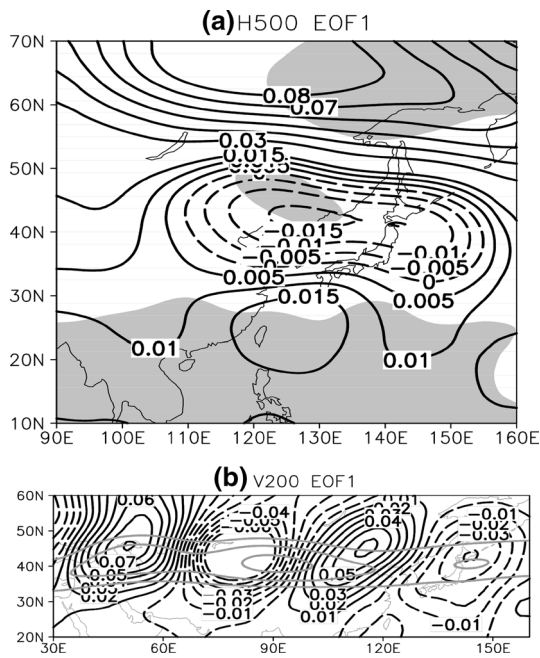


Fig. 1 Spatial pattern of the EOF1 for summer anomalies of **a** 500-hPa geopotential height (unit: gpm) over (10–70°N, 90–160°E) and **b** 200-hPa meridional wind velocity (units: ms^{-1}) over (20–60°N, 30–160°E) during 1981–2010. Gray lines in **b** denote 20 and 25 ms^{-1} contours of the climatological-mean zonal wind velocity, which indicate the Asian jet waveguide. Shadings in **a** indicate the 95% significance level of regression of 500-hPa geopotential height onto the first principle component

anomalies of summer geopotential height anomalies at 500-hPa during 1979–2015. This mode has a similar spatial characteristic to the EAP teleconnection (Huang 1987, 2004). In this pattern, summer geopotential anomalies are characterized by a meridional tripole anomalous pattern in the low-latitudes (20°N–30°N), mid-latitudes (35°N–50°N), and high-latitudes (55°N–70°N) region of EA–WP (Fig. 1a). Compared to the definition of PJ teleconnection (Nitta 1987), there is one more extended anomalous lobe located

in high-latitude region. The first spatial mode of EOF (with 25.2% contribution to total variance) of the summer meridional wind velocity at 200-hPa is shown in Fig. 1b, which indicates the SR teleconnection. The SR pattern is dominated by a quasi-stationary Rossby wave train in the upper troposphere along the summer Asian jet region (30°–50°N). The SR pattern has four anomalous lobes located at (50°E, 40°N), (80°E, 40°N), (110°E, 40°N), and (140°E, 40°N), respectively, which are consistent with the previous definitions (Enomoto et al. 2003; Ding and Wang 2005).

To reveal these teleconnection patterns more clearly, Fig. 2a presents the meridional cross section of these wave-like perturbations regressed onto the first principle component (PC1) of Fig. 1a. The regressed anomalies along 120°E exhibit a poleward wavelike pattern in the meridional direction. From the lower troposphere to the upper troposphere, positive anomalies with maximum amplitude are observed around 20°N and 70°N, while negative anomalies distribute around 40°N. This situation indicates that the wavelike pattern has an equivalent barotropic structure with slight northward tilting in the vertical direction. Statistically, significantly correlated regions further identify the tripole pattern is consistent with the EAP teleconnection in Fig. 1a, indicating that the EAP teleconnection has a deep vertical structure. The regressed zonal section of geopotential height onto the first principle component (PC1) of Fig. 1b is presented in Fig. 2b. The zonal cross-section along 40°E exhibits an obvious wave train structure with negative and positive anomalies aligned with the Asian jet waveguide. Two negative anomalies, with maximum amplitude observed around 30°E–60°E and 90°E–120°E, exhibit deep vertical structure tilting westward in the whole troposphere, while anomalous wave patterns within 60°–90°E are restricted mainly in the middle and upper troposphere. Statistically, significantly correlated regions also identify that this anomalous phase pattern is consistent with an eastward-propagating Rossby wave activity, suggesting that the SR teleconnection has the vertical structure. The stable vertical structures of EAP and

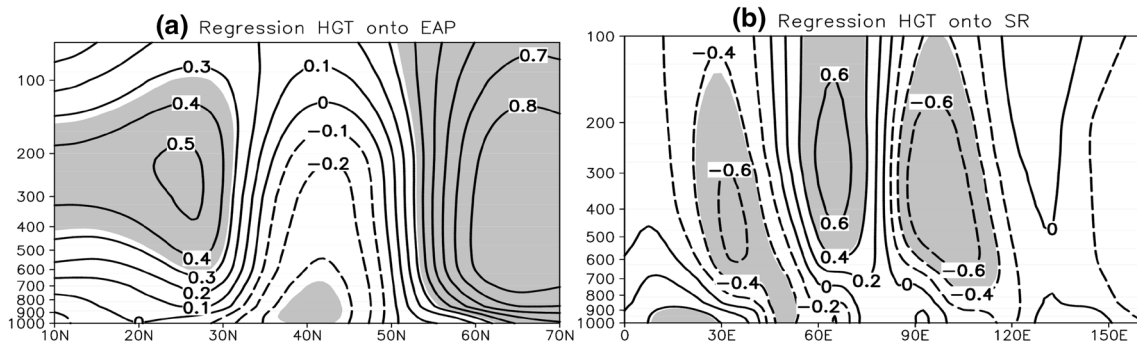


Fig. 2 **a** Meridional cross section of geopotential anomalies along 120°E regressed onto the PC1 of Fig. 1a and zonal cross section of geopotential anomalies along 40°N regressed onto the PC1 of Fig. 1b. Shaded areas indicate the 95% significance level

SR teleconnection, which are consistent with previous studies (Lu 2004, Hsu and Lin 2007; Kosaka et al. 2009), may cause certain co-action to the summertime atmospheric circulation and climatic anomalies in EA–WP.

In order to study the relationship between EAP and SR teleconnection (Huang 2004, Hsu and Lin 2007), indices of EAP teleconnection and SR teleconnection are defined by using the formula (1) and (2) in Sect. 2, respectively. Figure 3a shows composite differences of summer precipitation anomalies between five low-value years and five high-value years of EAP index. Negative precipitation anomalies with significant positive CCs distributed in tropical region (10°N–25°N) and extratropical region (50°N–70°N), while positive precipitation anomalies with significant negative CCs dominate the subtropical region (30°N–45°N) along the rainfall band from central East China to the Korean Peninsula, Japan and its maritime region. The spatial distribution of correlation between EAP and summer precipitation in EA–WP implies the similar meridional tripole pattern from low latitude areas to high latitude regions as EAP teleconnection. Composite differences of summer precipitation anomalies for SR index has an obvious zonal pattern along the 40°E longitude (Fig. 3b). Negative anomalies with

positive CCs dominate central East China, while positive anomalies with negative CCs control the region from the Korean Peninsula to Japan and its maritime region. The relationship between SR and summer precipitation may cause the latter’s zonal structure to align with the zonal direction wave pattern shown in Fig. 1b.

4 EAP and SR composition and related summer precipitation pattern and atmospheric circulation

Figure 4a presents the time series of EAP and SR indices, both are dominated by the interannual variation. Based on the two series, scatter distribution of EAP and SR (Fig. 4b) shows four patterns of EAP–SR composition, with anomalous phases as pattern I (positive EAP–positive SR, + +), pattern II (negative EAP–positive SR, – +), pattern III (negative EAP–negative SR, – –) and pattern IV (positive EAP–negative SR, + –), respectively. Table 2 presents corresponding years of different EAP–SR composition patterns. Year numbers for EAP–SR patterns vary from 6 to 11, implying the separation according to anomalous phase of EAP and SR index is meaningful. Therefore, these four patterns of EAP–SR composition can be used for further analysis of corresponding patterns of summer precipitation anomalies and atmospheric circulation anomalies in EA–WP.

Both EAP and SR teleconnections have obvious effect on the summer precipitation in EA–WP, which replace the westward expansion/eastward retreat of the PASH (Lu and Lin 2009; Kosaka et al. 2012) and influence moisture transport from the subtropics to the extratropics (Huang et al. 2007). Four patterns of summer precipitation anomalies and

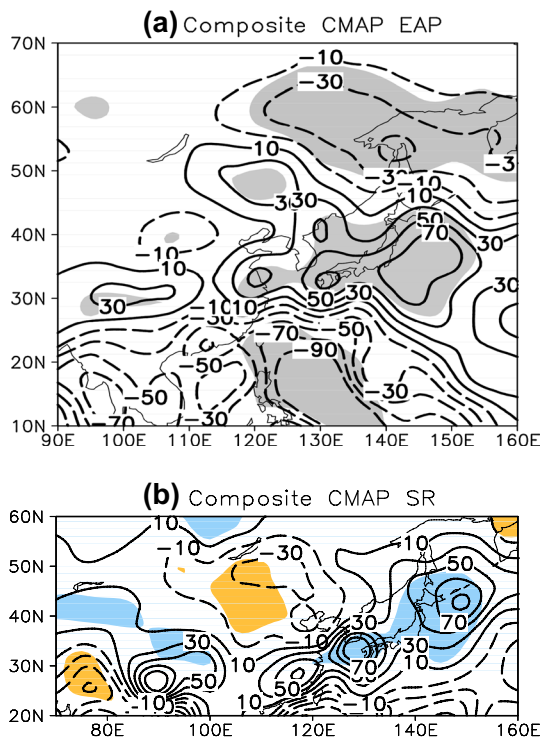


Fig. 3 Composites differences of summer precipitation anomalies (units, mm) between five low-value years and five high-value years for index of **a** EAP and **b** SR; Correlations (shading) of summer precipitation anomalies with index of **a** EAP and **b** SR, respectively. Correlation coefficients below the 95% significance level are not plotted

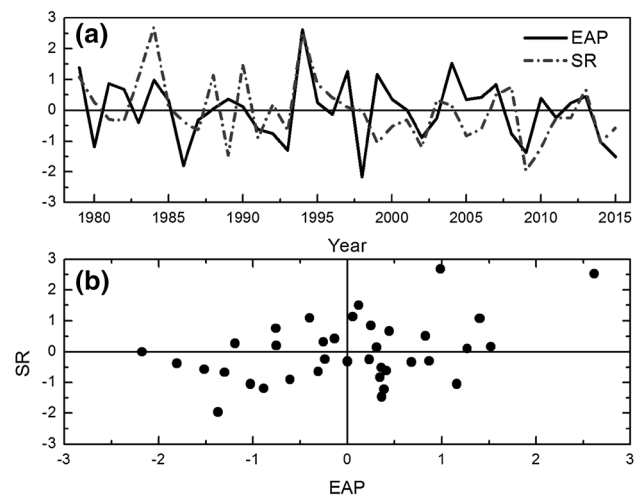


Fig. 4 EAP and SR curves **(a)** and scatter diagram indicating yearly distribution of EAP index and SR index **(b)**

Table 2 Years corresponding to different EAP–SR composition patterns

EAP–SR	Years
Pattern I (+ +)	1979, 1984, 1985, 1988, 1990, 1994, 1995, 1997, 2004, 2007, 2013
Pattern II (– +)	1980, 1983, 1992, 1996, 2003, 2008
Pattern III (– –)	1986, 1987, 1991, 1993, 1998, 2002, 2009, 2011, 2014, 2015
Pattern IV (+ –)	1981, 1982, 1989, 1999, 2000, 2001, 2005, 2006, 2010, 2012

“+” denotes positive index value, “–” denotes negative index value. Pattern I “+ +” denotes the EAP–SR composition with positive EAP index and positive SR index. Other three patterns have corresponding definitions as pattern I

500-hPa geopotential height anomalies corresponding to different EAP–SR compositions are exhibited in Figs. 5 and 6, respectively. Values larger than 0.5 standard deviations for both EAP and SR indices are selected to perform the composite analysis for Pattern I (III). Values larger than 0.3 standard deviations are selected for Pattern II (IV) because years that belong to these two patterns are less than the other two. Accordingly, 5 years (1979, 1984, 1994, 2007, and 2013) for pattern I, 4 years (1980, 1983, 2003, and 2008) for pattern II, 5 years (1991, 1993, 2002, 2009, and 2014) for pattern III and 7 years (1982, 1989, 1999, 2000, 2005, 2006, 2010) for pattern IV are selected respectively for composite analysis. For the pattern I, when summer precipitation is above normal in the tropical and extratropical region (Fig. 5a), negative anomalies of geopotential height at 500-hPa are obvious over the low latitude regions and high latitude regions of eastern EA–WP (Fig. 6a). Precipitation anomalies show west-east opposite phase over the subtropical region (Fig. 5a) accompanied by the positive-negative-positive wave like pattern from west to east along the 40°N zonal belt at 500-hPa geopotential height anomalies (Fig. 6a). For pattern II, summer precipitation anomalies show a tripole pattern with negative anomalies located in the tropical and extratropical regions and with positive anomalies distributed in the subtropical regions from west to east (Fig. 5b). Correspondingly, geopotential height anomalies at 500-hPa show the tripole pattern in meridional direction over EA–WP, while the west-positive east-negative pattern is replaced by the consistent negative anomalies along the band from lower reaches of the Yangtze river to Japan and the East regions (Fig. 6b). Composite differences of summer precipitation for pattern III–pattern I (Fig. 5c) have the similar spatial structure, but converse phase distribution of pattern I. Geopotential height anomalies in Fig. 6c correspondingly present the triple meridional structure along the band from North China to Japan, and exhibit a negative-positive-negative wave train from west to east along the 40°N zonal band over the subtropical regions. Composite differences of summer precipitation (Fig. 5d) and geopotential height (Fig. 6d) for pattern IV–pattern II exhibit a similar spatial structure of pattern II, but with converse phases anomalies. The summer precipitation composition modes of Pattern III

and pattern IV show significant correlation with the modes of pattern I and II, with the spatial CCs are respectively -0.59 and -0.33 , both passing the 99% significance level. That is to say, pattern III have the similar spatial structure but converse phase anomaly as pattern I.

Since four EAP–SR patterns are not totally independent from each other, the fraction variance percentage ($Var_{i,j}$) of each grid point is calculated as formula (5)

$$Var_{i,j} = \frac{\sum_{k=1}^N (R_k - \bar{R})^2}{\sum_{l=1}^M (R_l - \bar{R})^2} \times 100\% \quad (k = 1, 2, 3, \dots, N; l = 1, 2, 3, \dots, M) \quad (5)$$

where, R_k is the precipitation at each grid point, \bar{R} is the average precipitation for 1991–2015, l denotes the EAP–SR pattern, N is the number of years for each composition pattern, M is the total number of years from 1991 to 2015. The percentage variance for each pattern, (Var_L , $L = I, II, III, \text{ and } IV$), is calculated as the average for all the grid points within the region (10°N–70°N, 90°E–160°E). Percentage variance of summer precipitation explained by each of the four patterns are 12.5, 8.2, 8.0 and 19.6% respectively. Figure 7a, b show the relevant spatial features as those indicated in Fig. 5a, b, implying that the precipitation pattern defined by the EAP–SR composition is meaningful. As the spatial distribution of pattern III are respectively similar to the pattern I, the percentage variances figures are omitted. Therefore, it is possible that the major EA–WP summer precipitation variability can be represented by these four patterns, which are categorized based on the EAP–SR composite.

Geopotential height anomalies show a vertical wave pattern tilting slightly westward in the zonal direction over the subtropical region, exhibiting an equivalent barotropic structure for both pattern I and pattern II of EAP–SR compositions (Fig. 8a, c). Continuous negative (positive) anomalies in the zonal direction dominate the subtropical region for pattern II and pattern IV (Fig. 8b, d). Zonal cross-sections of vertical geopotential height anomalies averaged between 120°E and 130°E (Fig. 8e–h), demonstrate consistent tripole patterns between 30°N and 60°N,

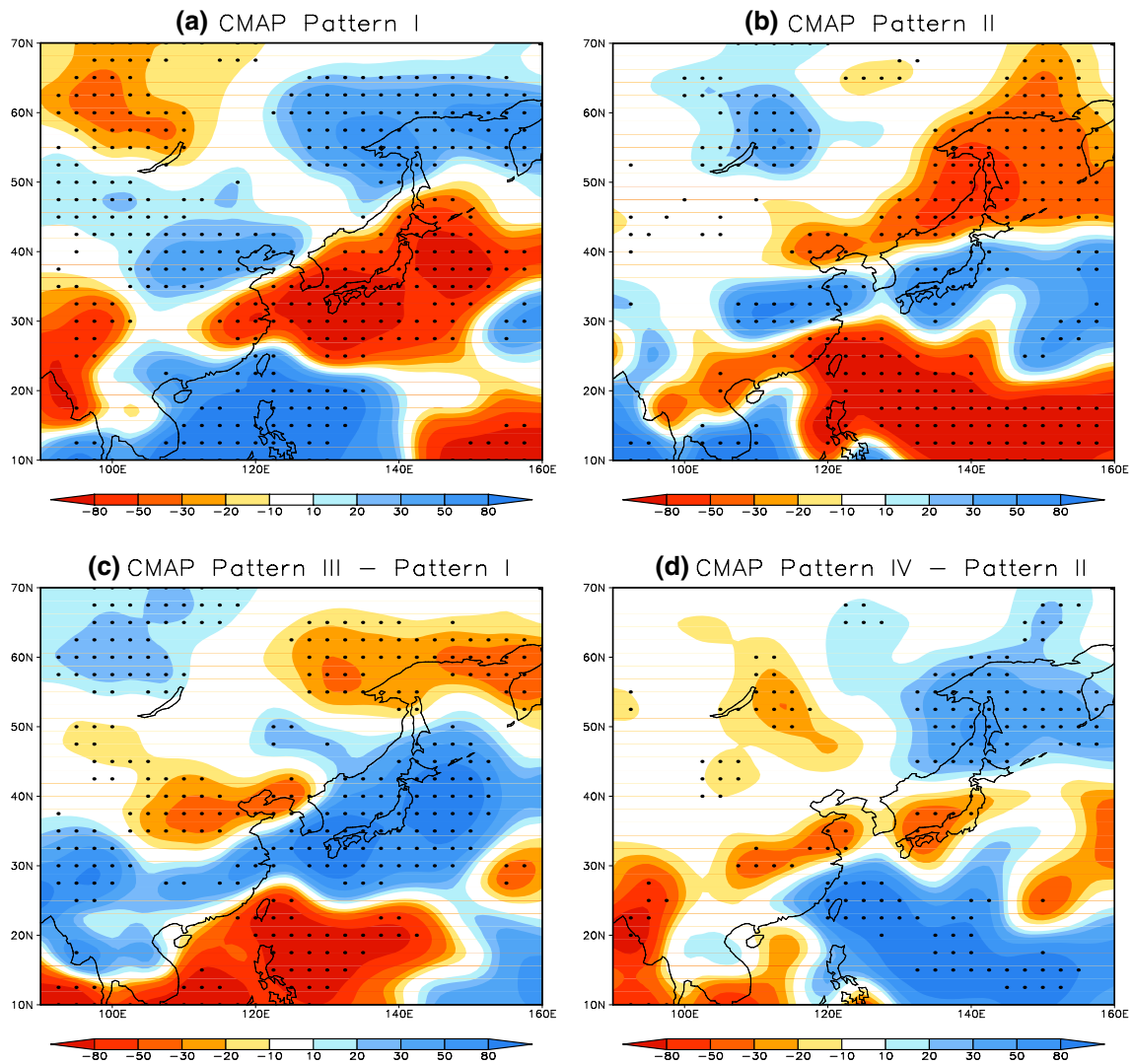


Fig. 5 Composed abnormal (units: mm) of summer precipitation for pattern I (a) and Pattern II (b) of EAP–SR composition; differences of composed abnormal (units: mm) for (c) pattern III–pattern I, (d) pattern IV–pattern II. Dotted areas indicate the 95% significance level

reflect that the anomalies over the subtropical region for pattern II are much weaker compared with pattern I (III).

Anomalies of 500-hPa wind vectors and integrated moisture divergence for EAP–SR patterns are presented in Fig. 9. For pattern I (Fig. 9a), wind anomalies at the middle troposphere (500-hPa) feature anomalous cyclones (anticyclone) over the tropical and the extratropical region (the subtropical region). These conditions, owing to the correlation of summer precipitation anomaly pattern with the anomalies of wind vectors and the moisture convergence (divergence) (Lu et al. 2006; Lu and Lin 2009; Xu et al. 2015), result in positive (negative) precipitation anomalies over the tropical and the extratropical regions (the subtropical region) of eastern EA–WP. Meanwhile, an anticyclone–cyclone–anticyclone–cyclone coupled wave train features the subtropical region from west to

east. The significant cyclone (anticyclone) over the West China (the North China–Japan region) leads to positive (negative) precipitation anomalies in North China (Japan and its maritime region). Composite differences of wind vectors and moisture divergence for pattern III–pattern I presented in Fig. 9c reflect that pattern III has the opposite spatial phase characteristics compared to pattern I. Meanwhile, for pattern II (Fig. 9b), wind vectors feature an anomalous anticyclone–cyclone–anticyclone meridional tripole pattern in the meridional direction, leading to the tripole anomalous precipitation distribution. The pattern I’s wave train over the subtropical region (Fig. 9a) is replaced by two cyclones controlling the western and eastern portions of the subtropical regions, which causes a positive precipitation band from the Yangtze River Basin to Japan. Figure 9d reflects that wind vectors and moisture

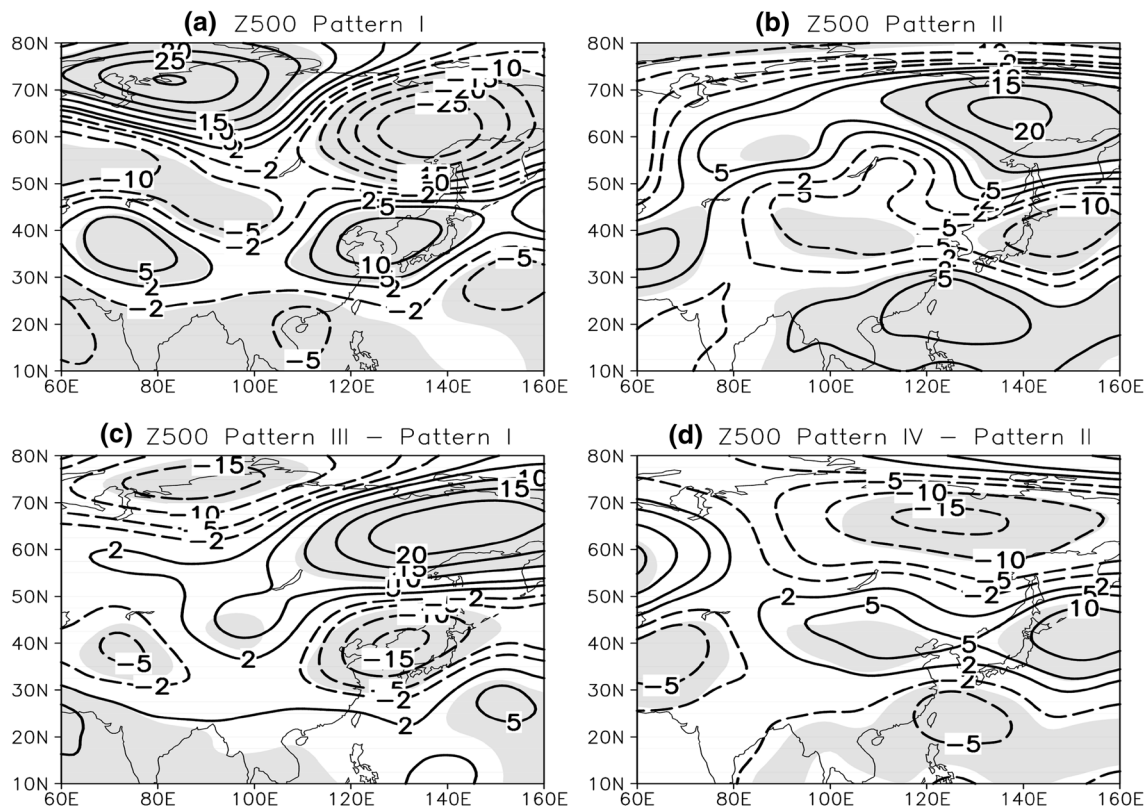


Fig. 6 Same as Fig. 5 but for composite anomalies of summer geopotential height (units: gpm) at 500-hPa. Shadings indicate the 95% significance level

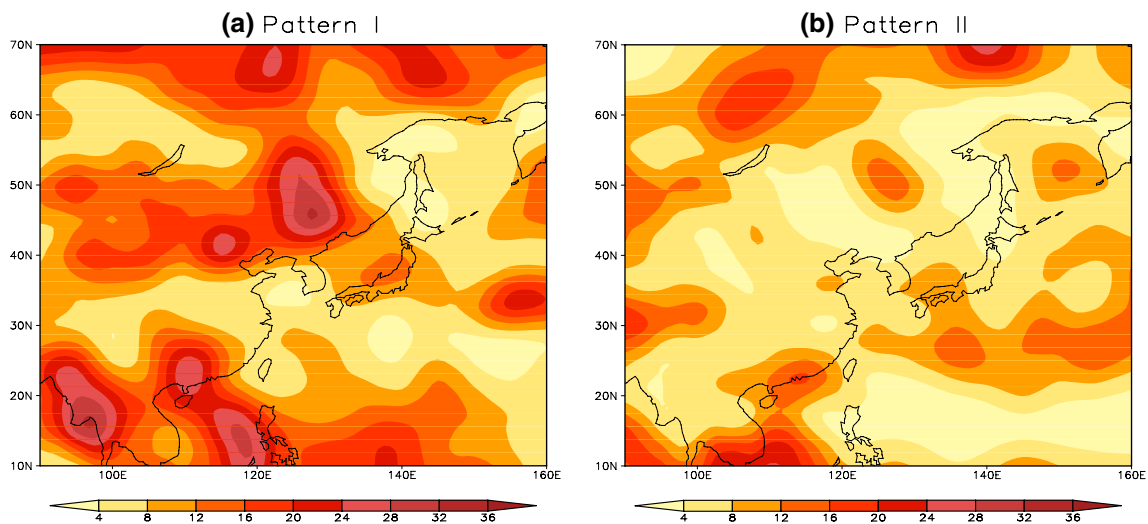


Fig. 7 Spatial distribution of percentage variance (unit: %) of summer precipitation for pattern I (a) and pattern II (b) of EAP-SR composition

divergence for pattern IV have the opposite spatial phase characteristics of pattern II.

Figure 10a, b are distributions of CCs of summer geopotential height anomalies with index of EAP and SR,

respectively. Negative CCs of EAP distribute in both tropical and extratropical regions, but positive ones in subtropical regions, reflecting the tripole structure in the meridional direction. CCs of SR feature positive-negative-positive

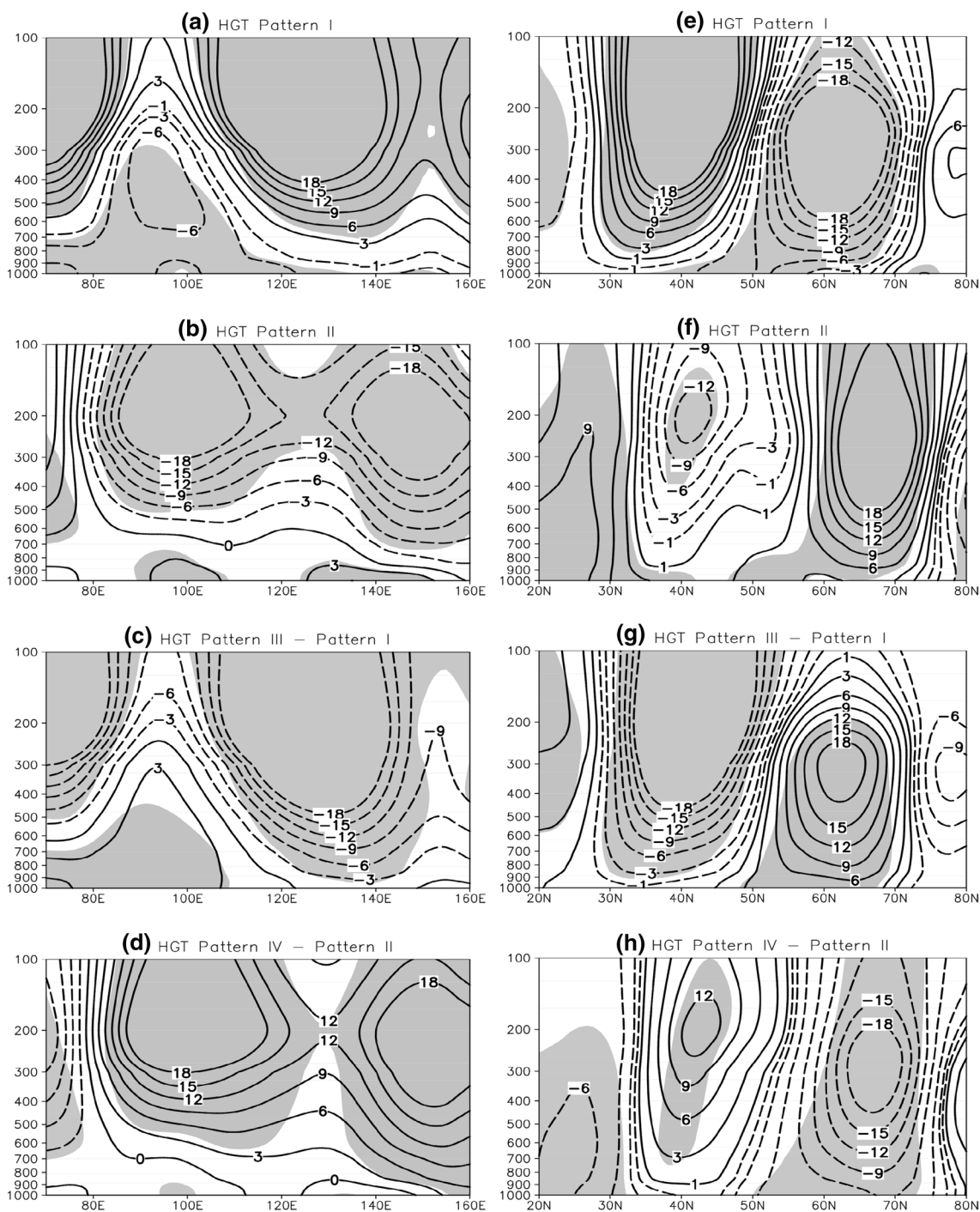


Fig. 8 Same as Fig. 5 but for the meridional cross-sections of geopotential (contour, gpm) along 40°N (a–d) and zonal cross-sections of average between 120°E–130°E (e–h) from 1000-hPa to 100-hPa. Shadings indicate the 95% significance level

values from 80°E to 130°E along the zonal direction of subtropical region. Since significantly correlated regions of EAP and SR overlapped in the Korean Peninsula, Japan and maritime regions, effect of EAP–SR compositions on the geopotential height at the 500-hPa level can be explained

by schematic diagrams of Fig. 10c, d. Pattern I of EAP–SR composition with positive–positive indices have a “+ – +” anomaly structure from west to east in the zonal direction and “– + –” anomaly structure from south to north in the meridional direction. The overlapped positive anomalies in

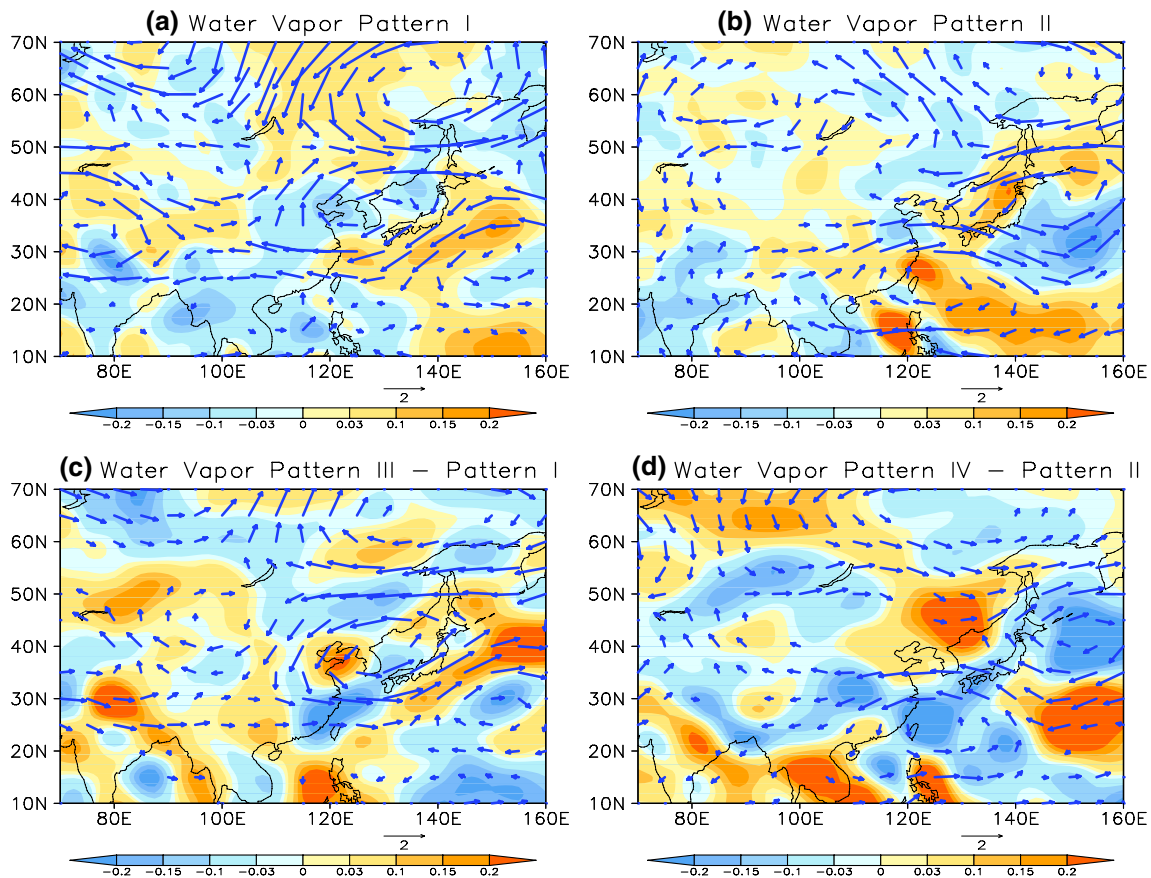


Fig. 9 Same as Fig. 5 but for divergence of integrated moisture from the surface to 200 hPa (shading, $10^{-5} \text{ kg m}^{-2} \text{ s}^{-1}$) and wind anomalies (vector, ms^{-1}) at 500 hPa. Only wind vectors above the 95% significance level are plotted

the subtropical region may strengthen the negative-positive anomalous phase contrast between the lobe east of and the lobe west of 120°E , and also strengthen the tripole anomalous structure in the meridional direction (Fig. 10 c), leading to the geopotential height pattern exhibited in Fig. 6a. Pattern III of EAP-SR composition with negative-negative indices has a similar explanation of pattern I. Fig. 10d shows pattern IV of EAP-SR composition with positive-negative indices, implying that the positive anomalous lobe of EAP in the subtropical region overlaps with the negative anomalous lobe of SR in the same region, which may weaken negative anomalies of SR and lead to the weak positive anomalies. Therefore, phase characteristics present two positive lobes in the zonal direction of the subtropical region (Fig. 6b). Meanwhile, negative lobes over extratropical and tropical regions respectively expand southward and northward, compressing the lobe over the subtropical region, causing the narrow and weak band of geopotential height anomalies. Pattern IV of EAP-SR composition shown in Fig. 6d can be explained with the similar mechanism as of pattern II.

5 The physical dynamics causes for EAP-SR compositions

5.1 The physical dynamics process of EAP teleconnection

The tropical western Pacific has the highest Sea Surface Temperatures (SSTs) around the global sea surface. Due to the dominant thermal states of this region, SSTs of the tropical West Pacific play an important role in triggering strong convective activity and convergence of air and moisture around the Philippines (Cornejo-Garrido and Stone 1977; Huang 1987; Nitta 1987; Ding 2007). Many studies (Kosaka and Nakamura 2006; Li et al. 2008) also show that EAP teleconnections are caused by the heating anomaly due to thermal anomalies of the tropical West Pacific, or by convective activity anomalies around Indonesia. The time series of the SST average for the Indonesia maritime continent (IMC, Indonesia and surrounding seas, $5^{\circ}\text{S}-5^{\circ}\text{N}$, $100^{\circ}\text{E}-130^{\circ}\text{E}$), within which SST anomalies are negatively correlated with the EAP index, is calculated.

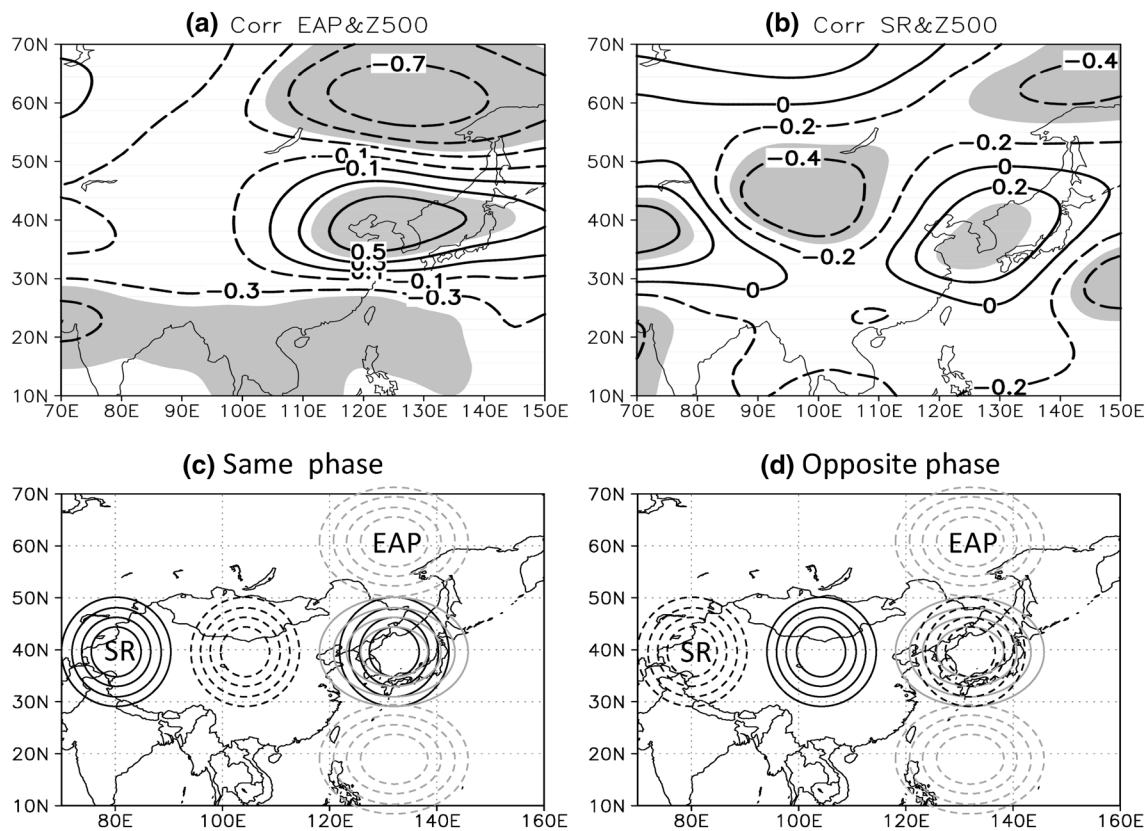


Fig. 10 Spatial distribution of CCs of geopotential height anomalies at 500-hPa with **a** EAP and **b** SR and the schematic diagram of the combination of EAP and SR teleconnections at 500-hPa with **c** same phase and **d** opposite phase. Shadings in **a**, **b** indicate the 95% sig-

nificance level. For the schematic diagrams, black lines and gray contours represent the EAP and SR teleconnection, respectively, while straight contours indicate positive anomalies and dash contours indicate negative anomalies

Regression anomalies of Outgoing Longwave Radiation (OLR) in Fig. 11a indicate that negative OLR dominates the tropical West Pacific, which may cause the anomalous convective heating and trigger the corresponding enhanced convective activity in this area. This enhanced convective activity causes an anomalous upward motion (Fig. 11b) and results in the cyclonic wind vector and positive vorticity anomalies at 850-hPa (Fig. 11c), and vice versa (Kosaka and Nakamura 2006). Meanwhile, positive OLR, downward motion, anticyclonic wind vector, and negative vorticity anomalies are observed over the SCS, which indicates that the positive geopotential height anomalies may dominate over this region. Meanwhile, negative OLR anomalies are observed around Japan and its maritime region (Fig. 11a), corresponding to enhanced convective activity (Fig. 11b) and positive geopotential height anomalies at 500-hPa. Corresponding to the significant meridional components, coupled vertical motions and horizontal wind anomalies from tropical region to extratropical region could be seen in Fig. 11b, c, indicating the interaction between different components of the tripole wave pattern. The regressed summer precipitation presents the positive-negative-positive-negative

spatial structure from the south to north (Fig. 11d) which is consistent with the OLR distribution shown in Fig. 11a. Therefore, thermal activity caused by anomalies of SSTs over the tropical West Pacific, especially over the IMC, might be one of the external forces for triggering the EAP teleconnection.

The composite OLR of pattern I indicates the meridional tripole structure from south to north and the zonal dipole structure along the 40°N, matching the precipitation distribution very well (Fig. 12a). It is also noted that the composite summer precipitation over the tropical region are different from the IMC SST regressed OLR (Fig. 11a) and precipitation pattern (Fig. 11d), implying there might be other factors that impact the EAP teleconnection. (Wang et al. 2009) suggested that the WNP monsoon trough convection over the Philippine Sea could be influenced by the ENSO, which may affect the summer WNP subtropical high and the rainfall pattern over EA through the EAP teleconnection. The tropical East SST regressed summer precipitation and OLR presents the similar structure as pattern I of EAP-SR composition, reflecting SST over the tropical East Pacific also plays an important role in triggering the EAP

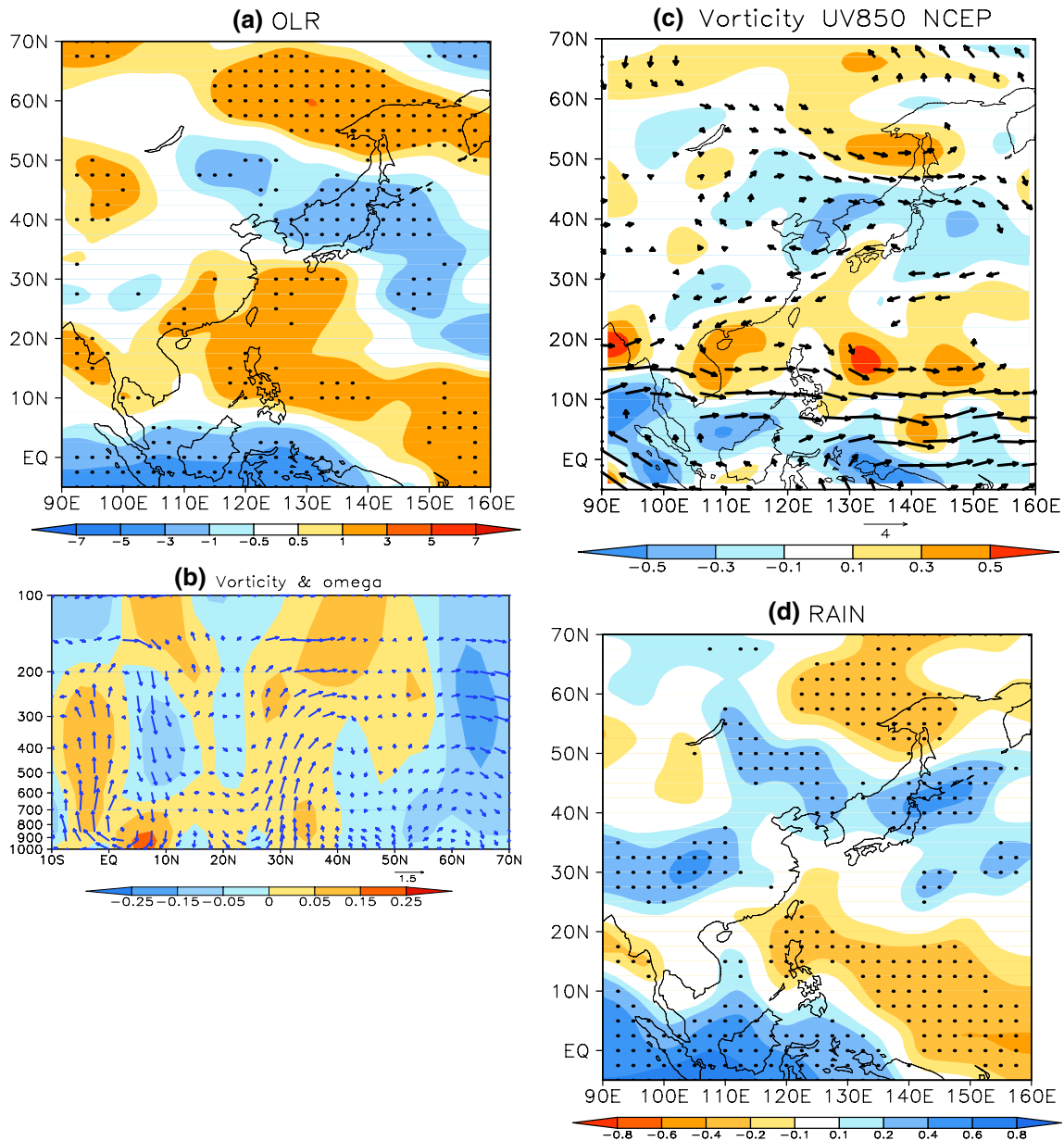


Fig. 11 Regression of anomalies of **a** OLR (units: $W m^{-2}$), **b** meridional cross-section of vorticity (shading, units: $\times 10^6 s^{-1}$) along 125°E and omega (vectors, $-0.01 Pa s^{-1}$) along 125°E from 1000-hPa to 100-hPa, **c** vorticity (shading, units: $\times 10^6 s^{-1}$) at 850-hPa (contour) and the corresponding wind vector (units: $m s^{-1}$), **d** standardized

summer precipitation onto the time series of the SST average for the Indonesia maritime continent (IMC, Indonesia and surrounding seas, 5°S–5°N, 100°E–130°E). Dotted areas in **a**, **d** indicate the 95% significance level, vectors of vertical motion below the 95% significance level in **c** are not plotted

pattern and influencing the relevant summer precipitation structure. Furthermore, the OLR of pattern II (Fig. 12b) shows the wave train structure in the meridional direction which is consistent with the IMC related OLR (Fig. 11a) and precipitation pattern (Fig. 11d), indicating the IMC related precipitation anomaly is comparable to the precipitation and OLR anomaly pattern. Accordingly, the remote tropical East SST forcing as well as the local SST forcing are both key

factors for producing the principle portion of summer precipitation over EA–WP (Zhou et al. 2009).

5.2 The atmospheric process of SR teleconnection

With respect to the SR teleconnection as a zonal wave train, Lu and Kim (2004) explained that this teleconnection may be due to the eastward propagation of the Rossby wave train along the westerly jet stream at 200-hPa. Kosaka et al.

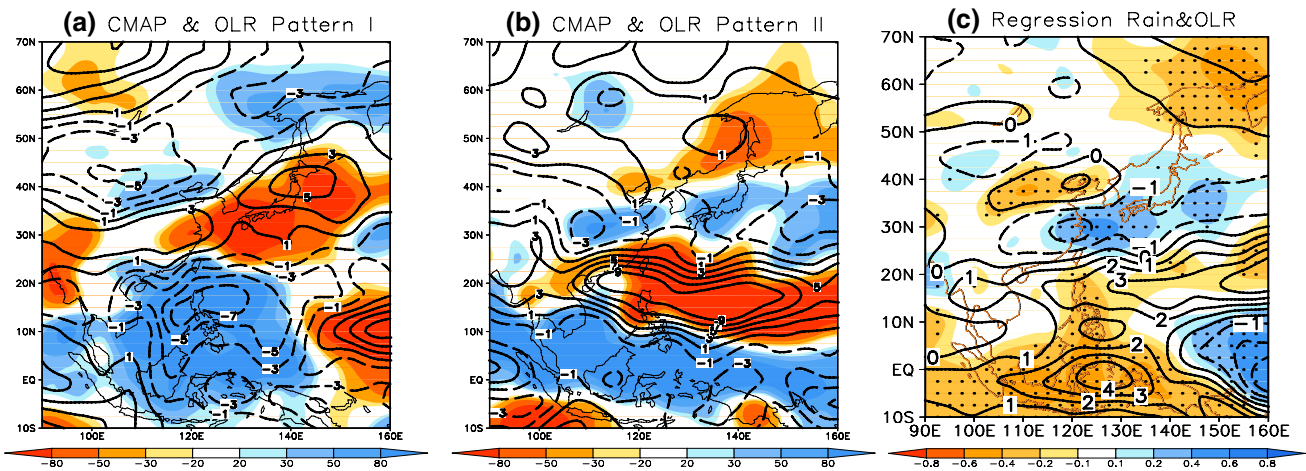


Fig. 12 Composite abnormal of summer precipitation (shading, units: mm) and OLR (contour, units: $W\ m^{-2}$) for **a** pattern I, **b** pattern II of EAP–SR composition, and regression of the standardized summer

precipitation and OLR onto the SST time series averaged over the tropical East Pacific region ($0\text{--}10^{\circ}N$, $90^{\circ}W\text{--}120^{\circ}W$), dotted areas in **c** indicate the 95% significance level for the summer precipitation

(2009) revealed that the SR’s extraction of available potential energy from the baroclinic Asian jet is highly efficient for its self-maintenance. Kosaka et al. (2012) further simulated that blocking developed over eastern Europe in 2010 was instrumental in triggering the SR teleconnection. Correlation between SR and meridional wind velocity anomalies at 200-hPa is shown in Fig. 13a. Significant correlation exhibits a wave pattern originating from Western Europe, extending to Japan along the Asian jet stream. The time series of the geopotential height anomalies averaged over the possible source of the SR teleconnection in East Europe ($37.5^{\circ}N\text{--}40.0^{\circ}N$, $60^{\circ}E\text{--}62.5^{\circ}E$) is defined as the EUGI index (EUGI). Meridional wind velocity anomalies regressed onto the EUGI (Fig. 13b) present a wave train pattern along the Asian jet stream. Regressed geopotential height anomalies and vorticity anomalies at 200-hPa (Fig. 13c) also show a similar wave train structure as the SR teleconnection.

It is also noted that a waveguide originates from Eastern Europe and propagates to Pakistan and northeastern India. According to a previous study (Ding and Wang 2005), an anomalous high can be triggered over Eastern Europe, causing a Rossby wave train propagation from western Europe to west-central Asia, resulting in an enhanced convection and precipitation over northwestern India and Pakistan. Figure 14 indicates that the MJJ (May, June, and July) precipitation may trigger the positive geopotential height and negative vorticity anomalies over central East Asia. Figure 15a, b show anomalies of Z200, vorticity, and meridional wind velocity at 200-hPa regressed onto the time series of the Z200 averaged over the central Asia ($37.5^{\circ}N\text{--}40^{\circ}N$, $60^{\circ}E\text{--}62.5^{\circ}E$), reflecting a wave pattern from West Asia to Japan. That is to say, strengthened Z200 over central West Asia could generate the SR teleconnection along the Asian

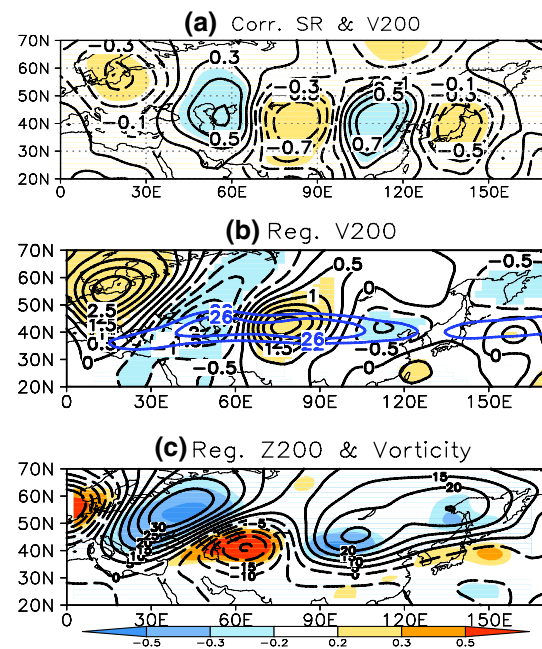


Fig. 13 Spatial distribution of **a** CCs of SR with meridional wind velocity anomalies, regression of **b** meridional wind velocity anomalies (contours, units: $m\ s^{-1}$) and vorticity anomalies (units: $10^{-6}\ s^{-1}$) and geopotential height (gpm) at 200-hPa onto the EUGI index. Shadings in **a**, **b** indicate the 95% significance level. Blue lines in **b** indicate the Asian jet; vectors of wave-activity flux below 0.5 in **c** are not plotted

jet stream. Figure 15c shows that MJJ precipitation over India and Pakistan could regress the wave train existed in the meridional wind field. Therefore, in combination with previous studies (Lu 2004; Ding and Wang 2005; Sato and Takahashi 2006; Kosaka et al. 2009; Lau and Kim 2012),

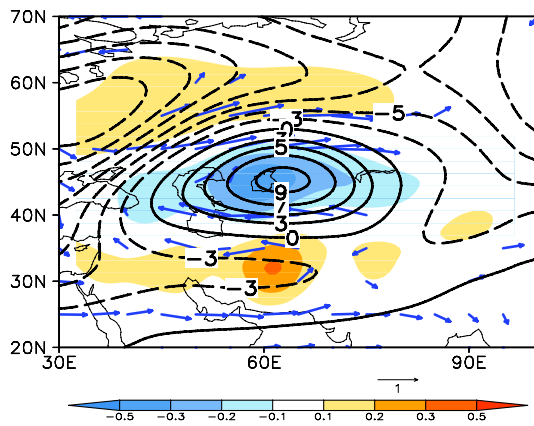


Fig. 14 Regression of summer (JJA) anomalies of Z200 (contour, units: gpm), vorticity (shading, units: $\times 10^6 \text{ s}^{-1}$) and wind velocity (vector, ms^{-1}) at 200-hPa onto the time series of the precipitation anomalies (MJJ) averaged over the region (18°N – 30°N , 65°E – 75°E). Vectors below the 95% significance level are not plotted

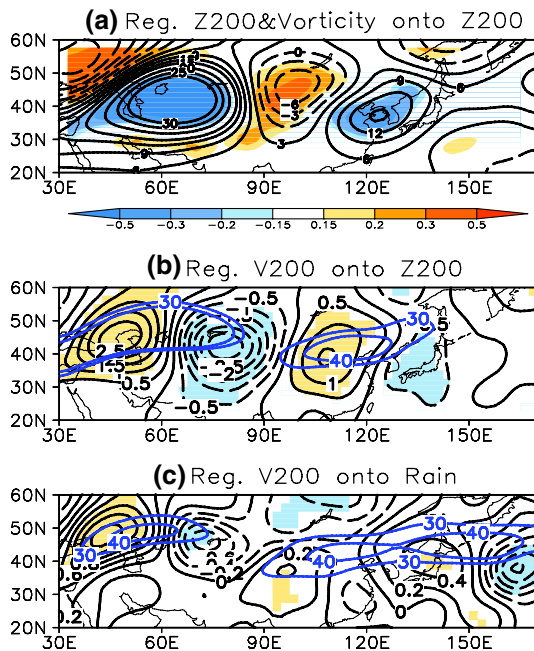


Fig. 15 Regression of anomalies of **a** Z200 (contour, units: ghm) and vorticity (shading, units: $\times 10^6 \text{ s}^{-1}$), and **b** meridional wind velocity (contour, units, ms^{-1}) at 200-hPa onto the time series of the Z200 averaged over the region (37.5°N – 40°N , 60°E – 62.5°E); **c** meridional wind velocity (vector, ms^{-1}) at 200 hPa onto the time series of the precipitation average over the region (18°N – 30°N , 65°E – 75°E). Blue lines in **b**, **c** are 30 and 40 ms^{-1} of contours of the climatological-mean zonal wind velocity, which indicate the Asian jet waveguide. Vorticity below the 95% significance level in **a** are not plotted. Yellow and blue shadings indicate the positive and negative 95% significance level

atmospheric anomalies in the upper troposphere over Eastern Europe might be the internal factor triggering the wave train propagation southwestward, causing the precipitation over Pakistan and northeastern India. The leading precipitation, in turn, strengthens the anomalous high over west-central Asia and then generates and maintains the SR teleconnection downstream.

6 SST anomaly and wave pattern corresponding to the EAP–SR composition

Section 4 revealed that anomalies of tropical Pacific SST is the major external force for exciting the EAP teleconnection, while the internal atmospheric anomalies and wave-activity are the major reasons for motivating and maintaining the SR teleconnection. The SST anomaly and wave-activity pattern corresponding to EAP–SR compositions are presented in this section.

Figure 16a shows the anomalies of SST corresponding to pattern I of EAP–SR composition, in which SCS, Bay of Bengal, the eastern tropical Indian Ocean and the tropical Pacific around the Philippines are dominated by negative SST anomalies. Meanwhile, negative SST is also observed in the tropical East Pacific. On the one side, as addressed in Sect. 4.1, negative SST anomalies over IMC suppress the convective activity in the tropical region, causing the anomalous upward motion and negative geopotential height at 500-hPa over the SCS through function of the Hadley circulation, then result in a positive EAP teleconnection. On the other hand, negative SSTs over tropical East Pacific may strengthen the convective activity in West Pacific, trigger the positive EAP and produce more precipitation in West Pacific

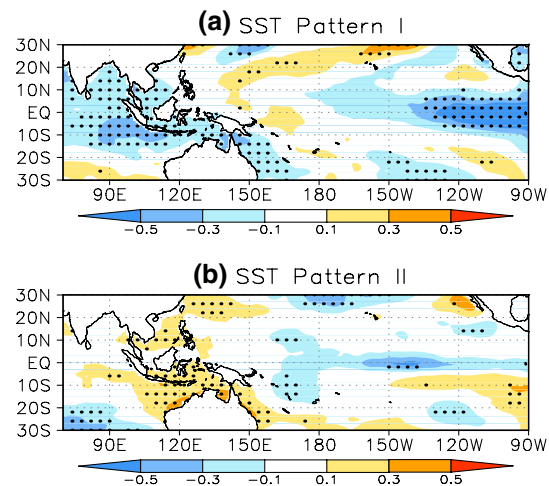


Fig. 16 Composite anomalies of SST (units: $^\circ\text{C}$) for **a** pattern I and **b** pattern II of EAP–SR composition. Shadings indicate the 95% significance level

(Fig. 12a). For pattern II of EAP–SR composition, positive SSTs anomalies over tropical East Pacific is not significant (Fig. 16b), indicating its weak tele-influence on West Pacific convection. Meanwhile, SSTs over IMC are dominated by positive SST anomalies (Fig. 16b), which can strengthen the heat convection, promote the anomalous upward motion at tropical region and cause the downward motion near the SCS through the Hadley circulation function, then lead to a negative EAP teleconnection and summer precipitation pattern presented in Fig. 12b. Therefore, the tropical East Pacific SST probably has a dominating impact on EAP teleconnection for pattern I, while the IMC SST plays an important role in influencing the EAP of pattern II. Pattern III (IV) of EAP–SR composition has the negative (positive) EAP phase as pattern II (I), the corresponding spatial distribution of SST anomalies is quite similar.

Figure 17a presents atmospheric anomalies and wave-activity flux of pattern I, in which eastern Europe is controlled by southward wind velocity anomalies and weak positive vorticity. Significant vorticity coupled with each other along the Asian jet stream, accompanied by eastward propagation of wave-activity fluxes, the meridional wind anomalies exhibit a “+–+–” pattern at 200-hPa from eastern Europe to Japan (Kosaka et al. 2012). Meanwhile, atmospheric anomalies and wave-activity flux of pattern IV are presented in Fig. 17b. Anomalies of meridional wind velocity and vorticity exhibit similar spatial structures but opposite anomalous phase of pattern I. Eastward wave-activity fluxes indicate the wave train may have originated from atmospheric anomalies over Eastern Europe, accompanied by a “+–+–” structure for meridional wind anomalies at

200-hPa. Since atmospheric circulation anomalies and wave-activity flux of pattern II (III), respectively, have similar anomalous structures as patterns I (IV), the spatial distribution figure is omitted.

7 Conclusion and brief discussion

EAP teleconnection has a close relationship with the meridional tripole pattern of summer precipitation over EA–WP, while SR teleconnection can affect the zonal anomalous wave pattern of summer precipitation along the Asian jet. Since origins of EAP and SR teleconnections are independent of each other (Huang 1987; Nitta 1987; Enomoto et al. 2003) and both teleconnections have influences on the climate of subtropical region, EAP–SR compositions are divided as pattern I (+ +), pattern II (+ –), pattern III (– –), and pattern IV (– +) based on EAP and SR indices for better understanding of the EAP–SR co-action on impacting climate anomalies in EA–WP.

Spatial distribution of summer precipitation over EA–WP for pattern I (pattern III) shows tripole meridional structure from low latitude to high latitude regions, with significant positive (negative) anomalies over tropical and extratropical regions, and negative (positive) anomalies over subtropical regions. This meridional tripole pattern is more distinct in the region east of 120°E than west of that longitude. The zonal precipitation anomalies of pattern I (pattern III) present west–positive (negative) and east–negative (positive) structure in subtropical region. Meanwhile, summer precipitation of pattern II EAP–SR composition also exhibits tripole structure in meridional direction, while the zonal structure over subtropical regions presents narrow but continuous positive (negative) anomalies along the band between 30–40°E.

Corresponding to the summer precipitation spatial anomalous distribution, geopotential height at 500-hPa shows the tripole meridional anomaly structure for pattern I (III) of EAP–SR composition, while the zonal anomalies along the Asian jet exhibit the “+–+” (–+–) wave pattern along the subtropical region from west to east. For pattern II, the meridional anomalous pattern at 500-hPa has a similar tripole structure, while the zonal wave pattern is replaced by the continuous negative (positive) anomalies over the subtropical region from the middle East China to Japan. Vertical sections of geopotential height anomalies further indicate that the EAP–SR composition maintains the atmospheric tripole anomalous pattern in the meridional direction. Besides, Pattern I (III) presents wave-like anomalous structure in the zonal direction over subtropical region of Eastern EA–WP, while pattern II (IV) exhibits continuous anomalies along the band around 40°N, with the anomaly intensity over subtropical regions being much weakened and anomaly belt

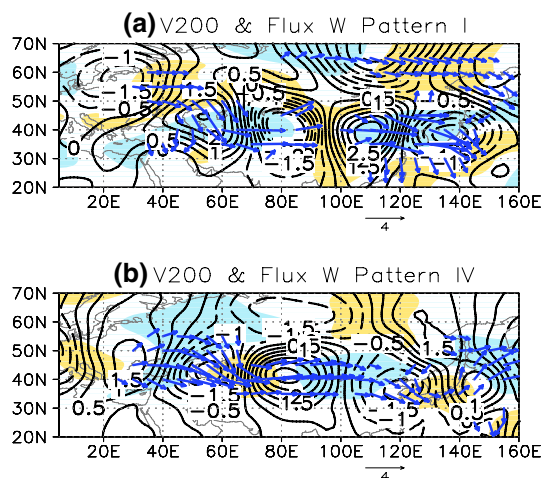


Fig. 17 Composite anomalies of summer meridional wind velocity (contours, units: ms^{-1}), vorticity (shaded, units: $\times 10^6 \text{ s}^{-1}$) and wave-activity flux (arrows, units: $\text{m}^{-2} \text{ s}^{-2}$) at 200-hPa level for **a** pattern I and **b** pattern IV of EAP–SR composition. Yellow shading indicates negative vorticity, while blue shading indicates positive vorticity. Vectors of wave-activity flux below 1.0 are not plotted

obviously compressed. It is implied that spatial distributions of geopotential height anomalies are consistent with the anomalous structure of summer precipitation in EA–WP. Moreover, spatial distribution of wind anomalies and moisture divergence (convergence) further demonstrate the possibility that summer precipitation patterns over EA–WP are caused by co-action of EAP and SR teleconnections.

The dynamical process of EAP teleconnection indicates that the thermal activity caused by anomalies of SST over the IMC is the external force for causing the EAP teleconnection. Meanwhile, atmospheric anomalies in the upper troposphere over eastern Europe might be the internal factor in causing wave train propagation to southward, triggering the precipitation over Pakistan and Northeastern India. The leading precipitation, in turn, will strengthen the anomalous high over west-central Asia that generates and maintains the teleconnection downstream of SR. Interpretation of the schematic mechanism for the co-action of EAP and SR teleconnection on influencing summer precipitation in EA–WP can be inferred in Fig. 18.

In Fig. 18a of pattern I, negative SST anomalies over tropical East Pacific may strengthen convective activity in the whole West Pacific, trigger the positive EAP teleconnection and produce more precipitation. Besides, the negative anomalies of SST over IMC can further weaken the thermal

convective activity, causing anomalous downward motion in equatorial region but upward motion over the SCS. The upward motion triggers negative anomalies in the middle troposphere (500-hPa) over low latitude regions through the function of Hadley circulation. Along with an equivalent barotropic structure tilting slightly northward, Rossby wave-like perturbations propagate northward in the lower and the middle troposphere, causing positive anomalies at 500-hPa over the subtropical regions. With the similar wave-activity propagating mechanism, negative anomalies dominate the high latitude region at 500-hPa. Meanwhile, in the zonal direction, positive anomalies at 500-hPa in Eastern Europe cause the wave-activity flux to propagate eastward along the Rossby wave train, which may also strengthen the precipitation over northeastern India and Pakistan. This situation causes the anomalous wave pattern “+−+−+” with positive SR teleconnection along the Asian jet stream at 500-hPa level. A positive SR-induced positive geopotential height anomalies over the Korean Peninsula and Japan overlapped with the positive lobe of EAP teleconnection, which may strengthen the west-negative and east-positive contrast anomalies across 120°E. Accordingly, pattern I of EAP–SR composition cause a meridional tripole pattern with more precipitation over low and high latitude regions, and less precipitation in subtropical regions in EA–WP. It also makes the zonal dipole pattern to exhibit more precipitation over central East China, but less precipitation over the Korean Peninsula, Japan, and maritime region. In pattern II (Fig. 18b), the SST anomalies over the tropical East Pacific is not significant, causing the weak tele-impact on the tropical West Pacific. Meanwhile, the negative anomalies of the IMC SST cause the negative EAP teleconnection. Corresponding negative anomalies over subtropical regions may weaken the positive SR-induced positive anomalies over the Korean Peninsula and Japan, leading to the continuous negative anomalies at 500-hPa over subtropical regions from central East China to Japan. Accordingly, more precipitation occurs over subtropical regions, while less precipitation exists over low latitude and high latitude regions in EA–WP. Pattern III of EAP–SR composition has a similar mechanism as Pattern I, while Pattern IV is similar to Pattern II.

Previous studies have also suggested that the mechanisms for triggering EAP teleconnection are diverse. For example, WPSH–ocean interaction can provide a source of climate predictability that extends ENSO impacts to upstream mid-latitudes, affecting the South Asian and EASM as a primary circulation system (Wang and Fan 1994; Wang et al. 2013). The PJ pattern is the atmospheric manifestation of an air–sea coupled mode spanning the Indo–NWP warm pool. The PJ pattern forces the Indian Ocean (IO) via a westward propagating atmospheric Rossby wave. In response, IO SST feeds back and reinforces the PJ pattern via a tropospheric Kelvin wave. Ocean coupling increases both the amplitude and

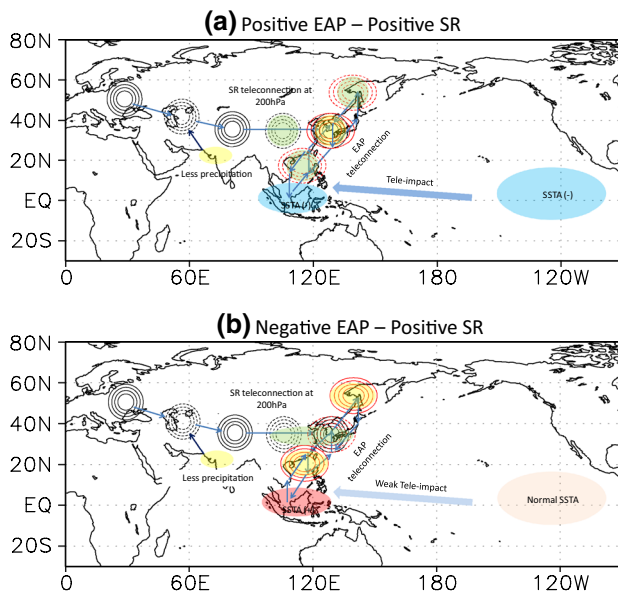


Fig. 18 Schematic diagram of the co-action of EAP and SR teleconnection on impacting the summer precipitation anomalous pattern over EA–WP. Black contours denote SR teleconnection at 200-hPa and red contours denote EAP teleconnection at 500-hPa. Arrows denote wave activity flux of Rossby wave train and vertical overturning circulation of EAP. Red shadings denote the positive SST anomaly, blue shading denotes the negative SST anomaly, green shadings denote more precipitation and yellow shadings denote less precipitation

temporal persistence of the PJ pattern (Kosaka et al. 2013). The North-West Pacific anticyclone (NWP-AC) is embedded in a large-scale meridionally anti-symmetric Indo-Pacific atmospheric circulation response and has been shown to exhibit large impacts on precipitation in Asia (Stuecker et al. 2015). In this paper, we focused our attention on the role of tropical West Pacific SSTs heating anomalies in exciting the EAP teleconnection through the function of tropical Hadley circulation. Therefore, local SST-induced convection could be argued as one of the explanations to the physical dynamics forming the EAP teleconnection. This study further confirms the theory proposed by (Wang et al. 2009), in terms of the origins, there are two categories of summer precipitation modes in EA: ENSO related and non-ENSO (or weak ENSO) related.

Acknowledgements The authors wish to thank anonymous reviewers' meaningful comments that led to a much-improved manuscript. Thanks also are extended to Dr. Pete Saunders for his great help in improving the writing of this manuscript. This work is supported by the National Natural Science Foundation of China (Grant Nos. 41575082, 41530531, and 41475064), the Special Scientific Research Project for Public Interest (Grant No. GYHY201306021).

References

- Chen G, Huang R, Zhou L (2013) Baroclinic instability of the silk road pattern induced by thermal damping. *J Atmos Sci* 70:2875–2893
- Cornejo-Garrido AG, Stone PH (1977) On the heat balance of the Walker circulation. *J Atmos Sci* 34:1155–1162
- Ding Y (2007) The variability of the Asian summer monsoon. *J Meteorol Soc Jpn* 85:21–54
- Ding Y, Chan J (2005) The East Asian summer monsoon: an overview. *Meteorol Atmos Phys* 89:117–142
- Ding Q, Wang B (2005) Circumglobal teleconnection in the Northern Hemisphere summer. *J Clim* 18:3483–3505
- Ding Q, Wang B, Wallace JM, Branstator G (2011) Tropical–extratropical teleconnections in boreal summer: observed interannual variability. *J Clim* 24:1878–1896
- Dogar MM, Kucharski F, Azharuddin S (2017) Study of the global and regional climatic impacts of ENSO magnitude using SPEEDY AGCM. *J Earth Syst Sci* 126:30
- Enomoto T, Hoskins BJ, Matsuda Y (2003) The formation mechanism of the Bonin high in August. *Q J R Meteorol Soc* 129:157–178
- Feng G, Zhao J, Zhi R, Gong Z (2013) Recent progress on the objective and quantifiable forecast of summer precipitation based on dynamical statistical method. *J Appl Meteorol Sci* 24:656–665
- Gong Z, Feng G, Ren F, Li J (2013) A regional extreme low-temperature event and its main atmospheric contributing factors. *Theor Appl Climatol* 117:195–206
- Gong Z, Feng T, Fang Y (2015a) Objective identification research on cold vortex and mid-summer rainy periods in Northeast China. *Chin Phys B* 24:049204
- Gong Z, Zhao J, Feng G, Chou J (2015b) Dynamic-statistics combined forecast scheme based on the abrupt decadal change component of summer precipitation in East Asia. *Sci China Earth Sci* 58:404–419
- Gong Z, Hutin C, Feng G (2016) Methods for improving the prediction skill of summer precipitation over East Asia–West Pacific. *Weather Forecast* 31:1381–1392
- Hoskins BJ, Karoly DJ (1981) The steady linear response of a spherical atmosphere to thermal and orographic forcing. *J Atmos Sci* 38:1179–1196
- Hsu H, Lin S (2007) Asymmetry of the tripole rainfall pattern during the East Asian Summer. *J Climate* 20:4443–4458
- Huang R (1987) Influence of the heat source anomaly over the tropical western Pacific on the subtropical high over East Asia. In: *Proceedings of international conference on the general circulation of East Asia*, April, pp 40–51
- Huang G (2004) An index measuring the interannual variation of the East Asian Summer Monsoon—the EAP index. *Adv Atmos Sci* 21:41–52
- Huang J, Yi Y, Wang S, Chou J (1993) An analogue-dynamical long-range numerical weather prediction system incorporating historical evolution. *Q J R Meteorol Soc* 119:547–565
- Huang R, Zhang Z, Huang G, Ren B (1998) Characteristics of the water vapor transport in East Asian monsoon region and its difference from that in South Asian monsoon region in summer. *Chin J Atmos Sci* 22:469–479
- Huang R, Chen J, Huang G, Zhang Q (2006) The quasi-biennial oscillation of summer monsoon rainfall in China and its cause. *Chin J Atmos Sci* 30:545–556
- Huang R, Chen J, Huang G (2007) Characteristics and variations of the East Asian monsoon system and its impacts on climate disasters in China. *Adv Atmos Sci* 24:993–1023
- Huang R, Chen J, Wang L, Lin Z (2012a) Characteristics, processes, and causes of the spatio-temporal variabilities of the East Asian monsoon system. *Adv Atmos Sci* 29:910–942
- Huang R, Liu Y, Feng T (2012b) Interdecadal change of summer precipitation over Eastern China around the late-1990s and associated circulation anomalies, internal dynamical causes. *Chin Sci Bull* 58:1339–1349
- Ishii M, Shouji A, Sugimoto S, Matsumoto T (2005) Objective analyses of sea-surface temperature and marine meteorological variables for the 20th century using ICOADS and the Kobe collection. *Int J Climatol* 25:865–879
- Kosaka Y, Nakamura H (2006) Structure and dynamics of the summertime Pacific–Japan teleconnection pattern. *Q J R Meteorol Soc* 132:2009–2030
- Kosaka Y, Nakamura H, Watanabe M, Kimoto M (2009) Analysis on the dynamics of a wave-like teleconnection pattern along the summertime Asian jet based on a reanalysis dataset and climate model simulations. *J Meteorol Soc Jpn* 87:561–580
- Kosaka Y, Chowdary JS, Xie S, Min Y, Lee J (2012) Limitations of seasonal predictability for summer climate over East Asia and the Northwestern Pacific. *J Clim* 25:7574–7589
- Kosaka Y, Xie SP, Lau NC, Vecchi GA (2013) Origin of seasonal predictability for summer climate over the Northwestern Pacific. *Proc Natl Acad Sci USA* 110:7574
- Lau WKM, Kim K-M (2012) The 2010 Pakistan Flood and Russian Heat wave: teleconnection of hydrometeorological extremes. *J Hydrometeorol* 13:392–403
- Li H, Dai A, Zhou T, Lu J (2008) Responses of East Asian summer monsoon to historical SST and atmospheric forcing during 1950–2000. *Clim Dyn* 34:501–514
- Li X, Wen Z, Zhou W, Wang D (2012) Atmospheric water vapor transport associated with two decadal rainfall shifts over East China. *J Meteorol Soc Jpn Ser II* 90:587–602
- Lu R (2004) Associations among the components of the East Asian summer monsoon system in the meridional direction. *J Meteorol Soc Jpn* 82:155–165

- Lu R, Lin Z (2009) Role of subtropical precipitation anomalies in maintaining the summertime meridional teleconnection over the western North Pacific and East Asia. *J Clim* 22:2058–2072
- Lu R, Li Y, Dong B (2006) External and internal summer atmospheric variability in the western North Pacific and East Asia. *J Meteorol Soc Jpn* 84:447–462
- Masao K, Wesley E, Jack W, Shi-Keng Y, J. HJ MF, L. PG (2002) Ncep-doe amip-ii reanalysis (r-2). *Bull Am Meteorol Soc* 83:1631–1643
- Nitta T (1987) Convective activities in the tropical western Pacific and their impact on the Northern Hemisphere summer circulation. *J Meteorol Soc Jpn* 65:373–390
- Nitta T, Hu Z (1996) Summer climate variability in China and its association with. *J Meteorol Soc Jpn* 74:425–445
- Qiao S, Gong Z, Feng G, Qian Z (2015) Relationship between cold winters over Northern Asia and the subsequent hot summers over mid-lower reaches of the Yangtze River valley under global warming. *Atmos Sci Lett* 16:479–484
- Sato N, Takahashi M (2006) Dynamical processes related to the appearance of quasi-stationary waves on the subtropical jet in the midsummer Northern Hemisphere. *J Clim* 19:1531–1544
- Stuecker MF, Jin FF, Timmermann A, McGregor S (2015) Combination mode dynamics of the anomalous Northwest Pacific Anticyclone. *J Clim* 28:1093–1111
- Takaya K, Nakamura H (2001) A Formulation of a phase-independent wave-activity flux for stationary and migratory quasigeostrophic eddies on a zonally varying basic flow. *J Atmos Sci* 58:608–827
- Wang B, Fan Z (1994) Choice of South Asian Summer Monsoon Indices. *Bull Am Meteorol Soc* 80:629–638
- Wang B, Wu R, Lau KM (2001) Interannual variability of the Asian summer monsoon: contrasts between the Indian and the Western North Pacific-East Asian Monsoons. *J Clim* 14:4073–4090
- Wang B, Jian L, Jing Y, Zhou TJ, Wu ZW (2009) Distinct principal modes of early and late summer rainfall anomalies in East Asia. *J Clim* 22:3864–3875
- Wang B, Xiang B, Lee JY (2013) Subtropical high predictability establishes a promising way for monsoon and tropical storm predictions. *Proc Natl Acad Sci* 110:2718–2722
- Webster PJ, Yang S (1992) Monsoon and ENSO: selectively interactive systems. *Q J R Meteorol Soc* 118:877–926
- Xu Z, Fan K, Wang H (2015) Decadal variation of summer precipitation over China and associated atmospheric circulation after the Late 1990s. *J Clim* 28:4086–4106
- Yang F, Lau KM (2004) Trend and variability of China precipitation in spring and summer: linkage to sea-surface temperatures. *Int J Climatol* 24:1625–1644
- Zhou T, Wu B, Wang B (2009) how well do atmospheric general circulation models capture the leading modes of the interannual variability of the Asian–Australian monsoon? *J Clim* 22:1159–1173

Affiliations

Zhiqiang Gong¹ · Guolin Feng¹ · Muhammad Mubashar Dogar^{2,3} · Gang Huang⁴

¹ Laboratory for Climate Studies, National Climate Research Center CMA, Beijing 100081, China

² Earth Science and Engineering, King Abdullah University of Science and Technology, Thuwal, Saudi Arabia

³ Global Change Impact Studies Centre, Ministry of Climate Change, Islamabad, Pakistan

⁴ Institute of Atmospheric Physics, Chinese Academy of Sciences, 100029 Beijing, China